ACS Catalysis

Research Article

pubs.acs.org/acscatalysis

Size and Promoter Effects in Supported Iron Fischer–Tropsch Catalysts: Insights from Experiment and Theory

Jingxiu Xie,[†] Jia Yang,[‡,∥] A. Iulian Dugulan,[§] Anders Holmen,[‡] De Chen,[‡] Krijn P. de Jong,*[,†] and Manuel J. Louwerse*[,†]

[†]Inorganic Chemistry and Catalysis, Debye Institute for Nanomaterials Science, Utrecht University, Universteitsweg 99, 3584 CG Utrecht, The Netherlands

[‡]Department of Chemical Engineering, Norwegian University of Science and Technology, Sem Saelands vei 4, N-7491 Trondheim, Norway

[§]Fundamental Aspects of Materials and Energy Group, Delft University of Technology, Mekelweg 15, 2629 JB Delft, The Netherlands

Supporting Information

ABSTRACT: The fundamentals of structure sensitivity and promoter effects in the Fischer–Tropsch synthesis of lower olefins have been studied. Steady state isotopic transient kinetic analysis, switching ^{12}CO to ^{13}CO and H_2 to D_2, was used to provide coverages and residence times for reactive species on supported iron carbide particles of 2–7 nm with and without promoters (Na + S). CO coverages appeared to be too low to be measured, suggesting dissociative adsorption of CO. Fitting of CH_4 response curves revealed the presence of parallel side-pools of reacting carbon. CH_x coverages decreased with increasing particle size, and this is rationalized by smaller particles having a higher number of highly active low coordination sites. It was also established that the turnover frequency increased with CH_x coverage. To calculate H coverages, new equations were derived to fit HD response curves, again leading to a parallel side-pool model. The H coverages appeared to be lower for bigger particles. The H coverage was suppressed upon addition of promoters in line with lower methane selectivity and higher lower olefin selectivity. Density functional theory (DFT) was applied on H adsorption for a fundamental understanding of this promoter effect on the selectivities, with a special focus on counterion effects. Na_2S is a better promoter than Na_2O due to both a larger negative charge donation and a more effective binding configuration. On the unpromoted Fe_5C_2 (111) surface, H atoms bind preferably on C after dissociation on Fe. On Na_2S-promoted Fe_5C_2 surfaces, adsorption on carbon sites weakens, and adsorption on iron sites strengthens, which fits with lower H coverage, less CH_4 formation, and more olefin formation.

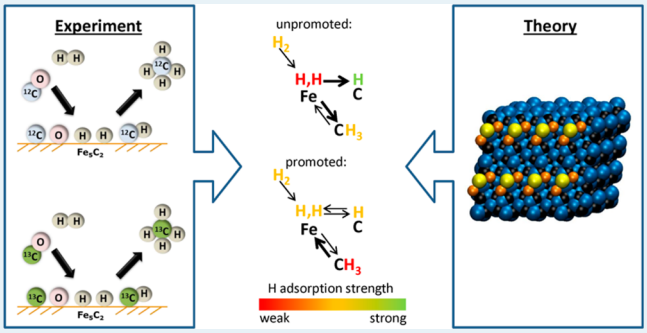

KEYWORDS: *Fischer–Tropsch, FTO, SSITKA, DFT, iron, lower olefins, synthesis gas, sodium, sulfur*

INTRODUCTION

Supported nanoparticles are used in various applications, including medicine, sensors, energy conversion and storage, optical devices, electronics, and heterogeneous catalysis.[1,2] In the latter, many reactions on such nanoparticles are structure sensitive.[3] Also, often small amounts of promoters are needed to obtain the desired activity, selectivity, or stability.[4] Size and promoter effects require much fundamental research to design good catalysts, with the notable example of Fischer–Tropsch (FT) synthesis.[5−7]

While iron, cobalt, and ruthenium are typical FT metals, iron[8] and cobalt[9] are preferred for production of lower olefins and high-molecular-weight paraffins, respectively. Lower olefins are basic building blocks which are used to produce a wide variety of products, ranging from plastics to pharmaceuticals. Although the traditional route to lower olefins production is thermal or catalytic cracking of naphtha or vacuum gas oil,[10,11] unconventional processes based on alternative feedstocks such as coal, natural gas, and biomass are of growing importance in recent years.[12−15] These alternative feedstocks may be converted to synthesis gas, a mixture of CO and H_2, to produce lower olefins, either indirectly via methanol[16,17] or dimethyl ether,[18] or directly via the Fischer–Tropsch to olefins (FTO) process.[8,19]

During the Fischer–Tropsch process many reactions occur simultaneously.[20−22] In essence, CO and H_2 reactant molecules dissociate, form CH_x species, and associate to form hydrocarbons via chain growth. Notably, on iron there is a competition between two types of termination reactions: H addition leading to alkanes versus β-H removal leading to

Received: January 14, 2016
Revised: March 29, 2016
Published: April 18, 2016

DOI: 10.1021/acscatal.6b00131
ACS Catal. 2016, 6, 3147−3157

olefins. Hence, a major challenge for the FTO process is the high methane selectivity. Addition of promoters, such as potassium, manganese, copper, and sulfur, has been shown to suppress methane formation.[23−26] Functionalization of carbon supports was also reported to promote the catalytic activity and selectivity toward lower olefins.[27−29] Especially effective is the combination of sodium and sulfur promoters, as was found by Torres Galvis et al.[30,31] Furthermore, upon addition of these promoters, the particle size of iron nanoparticles supported on carbon nanofibers (CNF) was discovered to play an instrumental role in increasing activity and selectivity toward lower olefins.[7]

In this work, the aim is to gain fundamental insights into the effect of iron particle size and of sodium and sulfur promoters. This is done experimentally with the steady state isotopic transient kinetic analysis (SSITKA) technique and with density functional theory (DFT) modeling.

In SSITKA, isotopic switches (^{12}CO to ^{13}CO and H_2 to D_2) are performed at steady state, after which the isotopic ratios in reactants and products are monitored with mass spectrometry (MS). The MS results are then analyzed to determine the surface residence times and surface coverages of reaction intermediates. SSITKA has been reviewed to be a suitable technique for kinetic study of heterogeneous catalytic reactions, including the iron FT synthesis.[32−34] Besides being used to understand the effect of activation methods, this technique was also used to investigate the effect of various promoters for iron FT catalysts at the active site level.[35−37] It was found for those promoters that higher catalytic activities relate primarily to increasing numbers of active surface intermediates. Recently, Govender et al. used SSITKA to propose mechanistic pathways for iron FT catalysts at a high temperature of 330 °C.[38−40] While iron catalysts were studied with SSITKA before, the effect of Na and S promoters and of iron particle size has yet to be investigated.

To gain even more fundamental understanding of the effects of the Na and S promoters, DFT modeling was used as well. While significant progress has been made on the theoretical understanding of the FT mechanisms on Co and Ru based systems, theoretical insights to the FT mechanism of Fe based systems are less complete.[41−43] This is due to the complex nature of the Fe catalyst, which includes the existence of different Fe phases and facets during FT reaction.[21,44−46] Most experimental and theoretical researchers accept that carburization is needed and χ-Fe_5C_2 is the most abundant active phase.[21] Due to the active phase being a carbide, it is further believed that a Mars−van-Krevelen-like mechanism occurs during FT reaction.[47,48]

Numerous theoretical calculations were performed.[49−52] Notably, Huo et al. found that the reaction energy of CH_4 formation on iron carbides is inversely proportional to the charge of the surface C atom.[53] This hints that promoters decrease the CH_4 selectivity in iron-catalyzed FTS by increasing the negative charge of surface carbon atoms. Modeling studies of potassium on iron and iron carbide also point to negative charge donations as the main promoter effect.[51,54,55] Here, the focus is on the combination of Na and S promoters, because the added effect of counterions is often not taken into consideration. Understanding why that combination is the best promoter found so far will also shed further light onto why lower olefin selectivity increased for promoted systems upon increase in particle size.

In the experimental samples, the weight loading of iron was varied between 2% and 20%, resulting in average iron carbide nanoparticle sizes of 2−7 nm. Catalytic tests were performed at methanation conditions (1.85 bar, 350 °C, H_2/CO = 10) to minimize the number of labeled products. Isotopic switches were subsequently carried out at steady state, and the response times of isotopic products were recorded. The transients of CH_4 and HD were fitted to various models, and fitting of HD transient curves was done for the first time.

EXPERIMENTAL METHODS

Catalyst Preparation and Characterization. *Preparation of Unpromoted Supported Catalysts.* CNF support was prepared as reported previously.[56] Four unpromoted catalysts with different iron loadings (2, 5, 10, 20 wt % Fe) were prepared using incipient wetness impregnation. A 7.014 g portion of ammonium iron citrate (Fluka, purum p.a., 14.5−16 wt % Fe) was dissolved in 25 mL of demineralized water to form a stock solution. Except for the 2 wt % Fe loaded catalyst, every catalyst required successive impregnation steps. The samples were dried under static air at 120 °C between impregnation steps and after the final impregnation step for 1 and 2 h, respectively. Calcination was performed at 500 °C for 2 h under nitrogen flow (5 °C/min; 100 mL/min for 2 g catalyst). After cooling to room temperature, the catalyst was passivated by oxidation. The oxygen concentration was increased stepwise (2% v/v increase every 30 min) until reaching 20% v/v. The number in the sample code indicates the nominal iron loading.

Preparation of Promoted Supported Catalysts. Four promoted catalysts with different iron loadings (2, 5, 10, 20 wt % Fe) were prepared using incipient wetness impregnation. A 6.954 g portion of ammonium iron citrate (Fluka, purum p.a., 14.5−16 wt % Fe), 0.199 g of sodium citrate tribasic dihydrate (Sigma-Aldrich, >99.0%), and 0.056 g of iron(II) sulfate heptahydrate (Merck) were dissolved in 25 mL of demineralized water to form a stock solution. Subsequent steps were performed as described above. In addition to the number in the sample code which indicates the nominal iron loading, the letter P was included for promoted catalysts.

Characterization. Iron, sulfur, and sodium contents in the samples were analyzed with ICP-OES (inductively coupled plasma−optical emission spectroscopy) using a Spectro Ciros CCD spectrometer. Transmission electron microscopy (TEM) images were attained on a Philips Tecnai-20 FEG (200 kV) microscope equipped with an EDX and an HAADF detector. The average iron oxide particle sizes were in agreement with those reported in a previous publication.[7] The composition of the Fe phases before reaction, after reduction, and after FTO reaction was determined in situ with transmission ^{57}Fe Mössbauer spectroscopy. Transmission ^{57}Fe Mössbauer absorption spectra were collected at 300 K with a conventional constant-acceleration spectrometer using a $^{57}Co(Rh)$ source. Velocity calibration was carried out using an α-Fe foil. The Mössbauer spectra were fitted using the Mosswinn 4.0 program. The Mössbauer transmission cell has a tubular reaction chamber with an internal diameter of 15 mm, and the catalyst bed lengths were 1.5−3 mm (catalyst loading of 100−300 mg). Although the reactant gases pass through the catalyst bed, the Mössbauer cell is not a plug-flow reactor due to a large dead volume (~7 cm^3) before the catalyst bed. A total flow rate of 100 mL/min was used during treatments, corresponding to a gas hourly space velocity (GHSV) of about 12000−24000 h^{-1}.

DOI: 10.1021/acscatal.6b00131
ACS Catal. 2016, 6, 3147−3157

The reaction conditions were as described in the transient isotope experiments below.

Transient Isotope Experiments. The SSITKA setup used was described in other publications.[57] The quantity of catalyst loaded was varied to achieve CO conversion of approximately 10%. For promoted catalysts, 150 mg of catalyst (212−425 μm) was diluted with 300 mg of SiC (212−425 μm) and loaded in a plug flow U-shaped reactor. For unpromoted catalysts, catalyst loading was varied between 75 and 400 mg. The catalysts were first reduced in situ for 2 h at 350 °C (ramp 5 °C/min) and 1 bar under diluted H_2 flow (H_2 /Ar = 20/40 mL/min). After reduction, the temperature was kept at 350 °C, the pressure was raised to 1.85 bar, and diluted synthesis gas ($^{12}CO/H_2$ /Ar = 0.75/7.5/16.75 mL/min) was introduced. The SSITKA experiment was performed after 20 h of reaction to arrive at relatively stable performance (steady state).

The performance of the catalysts was monitored online with an HP5890 gas chromatograph (GC) equipped with FID and TCD. The activity of the catalyst, specifically CO conversion, and the selectivity (excluding CO_2) were calculated from TCD and FID chromatograms, respectively.

Upon reaching steady state, an isotopic switch from $^{12}CO/H_2$ /Ar to $^{13}CO/H_2$ /Kr was performed, and these isotopic transient responses were monitored with a Balzers QMG 422 quadrupole mass spectrometer. The isotopic switch from CO/H_2/Ar to CO/D_2/Kr was also carried out. Usually the average surface residence time (τ) is determined from the area under the normalized transient curve (Figure 1), using the Ar or Kr

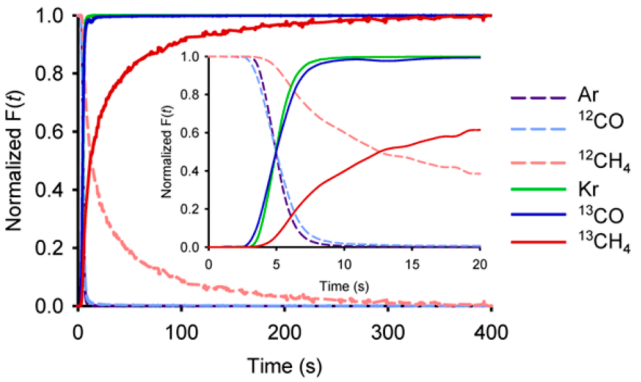

Figure 1. Typical normalized transient curves of full period and initial period (inset) from a $^{13}CO/H_2/Kr$ to $^{12}CO/H_2/Ar$ backswitch (catalyst 2PFeCNF).

inert tracer to correct for gas phase hold-up.[57] Correction for a chromatographic effect of CO was not necessary here. However, fitting of the hold-up-corrected CH_4 response curves to the models of Soong et al. revealed the presence of parallel carbon pools, resulting in a τ_1 and a τ_2.[58]

Different types of parallel pool models give identical fitted curves but different relations between τ_1 and τ_2.[58] Here, the parallel side-pool model was considered most appropriate. The surface coverage, θ, of CH_x species (main-pool) was calculated by dividing the number of adsorbed CH_x species (N_{CHx}) by the number of Fe surface atoms. N_{CHx} was determined by multiplying τ_1 and the exit flow, Q, of CH_4. The number of Fe surface atoms was calculated assuming that the particles consist fully of Fe_5C_2. From the density of Fe_5C_2 (ρ = 7.57 g/mL), it was calculated that there were 75 Fe atoms/nm^3 and 17.8 Fe atoms/nm^2.

$$\theta_{CH_x} = \frac{\tau_1 Q_{CH_4}}{N_{\text{Fe surface atoms}}}$$

To determine H coverage, HD response curves were fitted as well. For this recombined species, new equations were derived on the basis of the equations of Soong et al.[58] These new equations do differ between normal parallel pools and parallel side-pools ($\theta_{H,1}\theta_{D,1} + \theta_{H,2}\theta_{D,2}$ vs $\theta_H\theta_D$, respectively) and the parallel side-pool (model D) was found to give the best fits. Since HD curves were normalized with respect to H_2 curves and exiting H_2 could be both recombined or unreacted H_2, a conversion factor, χ, was included. θ' values are normalized coverages:

$$\theta'_H(t) = \chi^{1/2}(Ae^{-t/\tau_\alpha} + (1-A)e^{-t/\tau_\beta})$$

$$\theta'_D(t) = \chi^{1/2} - \theta'_H(t)$$

$$[HD](t) = 2\theta'_H(t)\theta'_D(t)$$

The relationship between τ_α and τ_β, and τ_1 and τ_2, was shown in detail in ref 58. Once τ_1 was found, the absolute H coverage was calculated:

$$\theta_H = \frac{\tau_1 \chi^2 Q_{H_2}}{N_{\text{C surface atoms}}}$$

From the modeling studies performed in this work, it was concluded that H surface species reside preferentially on C rather than on Fe atoms of the Fe_5C_2 surface. Hence, the surface coverage of H was calculated by dividing the number of adsorbed H atoms by the number of C surface atoms. From the density of Fe_5C_2, it is calculated that there are 30 C atoms/nm^3 and 9.7 C atoms/nm^2.

For the calculation of surface coverages, the active surface was calculated from the Fe_5C_2 particle sizes reported in Table 1.

Table 1. Properties of Promoted and Unpromoted CNF-Supported Iron Catalysts

	wt % loading[a]			av particle size (nm)	
	Fe	Na	S	Fe_2O_3[b]	Fe_5C_2[c]
CNF support	N.D.	0.4	<0.01	N.A.	N.A.
2FeCNF	2.2	0.6	<0.01	2.7	2.2
5FeCNF	4.3	0.5	<0.01	4.0	3.2
10FeCNF	6.9	0.5	0.01	6.9	5.5
20FeCNF	15.0	0.5	<0.01	8.6	6.9
2PFeCNF	2.2	0.6	0.02	2.7	2.2
5PFeCNF	4.6	0.6	0.03	4.1	3.2
10PFeCNF	8.4	0.6	0.06	6.8	5.4
20PFeCNF	13.9	0.6	0.11	8.7	7.0

[a]Measured with ICP-OES. [b]Number-average determined by TEM. [c]Calculated from TEM data of Fe_2O_3.

However, as reported in ref 7 and confirmed by analyzing spent catalyst 20PFeCNF, the particles may grow by 10−40% due to sintering, decreasing the active surface by the same percentage. On the other hand, as mentioned below, carburization is only partial and likely progressing from the surface inward,[59,60] leading to core−shell particles that are only slightly smaller than the original Fe_2O_3 particles, causing us to underestimate the active surface by roughly 20%. Since these two sources of uncertainty more or less negate each other, we choose to ignore them for the sake of simplicity.

DOI: 10.1021/acscatal.6b00131
ACS Catal. 2016, 6, 3147−3157

Table 2. Catalytic Performance of Catalysts at Methanation Conditions (1.85 bar, 350 °C, H_2/CO = 10, TOS = 15 h)

	FTY (10^{-6} mol_{CO}/g_{Fe} s)	apparent TOF[d] (10^{-3} s^{-1})	product selectivity (% C)			
			CH_4	C_2-C_4 olefins	C_2-C_4 paraffin	C_{5+}
2FeCNF	36.6	20.5	64	23	11	2
5FeCNF	1.2	0.9	68	19	12	1
10FeCNF	1.4	2.0	72	15	12	2
20FeCNF	0.7	1.2	70	21	7	2
2PFeCNF	20.1	9.1	55	21	22	3
5PFeCNF	5.8	4.4	47	33	16	4
10PFeCNF	3.4	4.8	40	41	16	4
20PFeCNF	1.4	2.4	34	50	11	6

[d]Apparent turnover frequency: moles of CO converted to hydrocarbons per mole of surface Fe per second.

DFT Modeling. DFT modeling was performed with the ADF-BAND package (version 2014.04),[61,62] using the rPBE functional[63] and Grimme D3 corrections[64] with Becke–Johnson damping.[65] The rPBE functional was chosen since we are modeling surface adsorption; dispersion corrections are needed for proper adsorption of sulfur species. A TZP basis set (TZ2P for sulfur) with small frozen cores, a "normal" kspace (kpoints up to at least 10 Å), a "normal" Becke grid, and "good" zlm-fit parameters were used. For efficiency, the SCF was converged to only 5×10^{-4} Hartree, and the tails of the orbitals were ignored below 10^{-4} Hartree; and the old gradient routine was used and converged to 0.004 hartree/Å. All settings were tested to be appropriate.

Before modeling the catalyst surface, bulk Fe_5C_2 was reoptimized with these settings. The resulting unit cell dimensions were the following: a = 11.29 Å, b = 4.39 Å, c = 4.91 Å, and β = 97.4°, ca. 3% shorter in each direction than that typically obtained without Grimme corrections.[44,45] The magnetic moment was 1.76 μ_B, which is typical.

The Fe_5C_2 surfaces were modeled according to the work of Zhao and Jiao et al., who determined the most stable surfaces and surface terminations under Fischer–Tropsch conditions.[45] After correcting their Wulff construction, the most abundant surface was found to be the (111) surface.[66] We have assumed that the same termination of the (111) surface is most stable and abundant when there are promoters present on the surface.

The surface calculations were performed with slabs of 9 Å thick and the atoms in the bottom 3 Å frozen. For efficiency, the frozen atoms were calculated with minimal settings (SZ basis sets with large frozen core, orbital confinement to 4 bohr, and "basic" settings for the Becke grid and zlm-fit parameters). Surface calculations were performed on 2 × 2 unit cells, implying supercell vectors of 12.11 and 13.17 Å with an angle of 98.7°. Since the ADF-BAND uses true 2D periodicity, no vacuum spacing nor dipole corrections were needed.

We studied the adsorption of Na, NaOH, NaSH, Na_2O, and Na_2S on the (111) surface of Fe_5C_2. Often, only adsorbed alkali atoms are modeled, but here purposely the effect of the counterions was studied as well, focusing on the effect of the promoters on the adsorption of H atoms. H adsorption on carbon sites versus H adsorption on iron sites is related to CH_4 (H_2 dissociates on Fe and H moves to carbon)[45] versus olefin formation (a hydrogen returns to iron). First, optimal positions for Na, NaOH, NaSH, and H were determined on a 1 × 1 unit cell by running optimizations from a grid of 25 starting positions above the surface (times 4 orientations for NaOH and NaSH). The most favorable positions were recalculated on the 2 × 2 unit cell. For Na consistently the two most favorable positions were found, and these were used to construct eight possible structures each for Na_2O and Na_2S.

For the two most favorable positions for each promoter, the effect on the adsorption of H at its preferred positions was studied. In fact, due to the asymmetry introduced by the presence of one promoter species per four unit cells, each H position now has four unique duplicates in neighboring unit cells. Note that each of these four duplicates has a different distance to the promoter species. Out of the four duplicates at least the closest and the furthest were calculated for each H position and for each promoter geometry, but excluding structures with obvious sterical clashes.

Atomic charges were calculated with Hirshfeld's method.[67] It should be kept in mind that these charges are only indicative (as with any charge assignment scheme), since atoms overlap and therefore atomic charges are ill-defined. Adsorption energies of H atoms were calculated with respect to $1/2H_2$ (g).

RESULTS AND DISCUSSION

An overview of the catalysts and their properties is presented in Table 1. It is noted from ICP elemental analysis results that the unpromoted catalysts contained some sodium, as well. However, this is assumed to be present on the support and to not affect the iron nanoparticles. For sulfur, assuming all sulfur resides on the iron carbide surface and the coverage of terraces and edges is equal, the implied coverage ranges from 3% to 14%.

Since previous catalytic tests[7] were performed at FTO conditions (H_2/CO = 1), the catalytic performance at methanation conditions (H_2/CO = 10) needed first to be established. Despite the differences in reaction conditions, similar trends were observed for the catalytic performances (Table 2 and S2 in the Supporting Information): For the unpromoted catalysts, methane was the dominant product, whereas the promoted catalysts showed relatively low selectivity to methane. Also, the trend with respect to particle size was similar as found previously at FTO conditions.[7]

In situ Mössbauer spectroscopy was performed to compare the composition of Fe phases at FTO[7] and methanation conditions (S1 in the Supporting Information). It was shown that partial carburization (~20%) was attained for all catalysts. While absolute composition of Fe phases varied between FTO and methanation conditions, similar trends were found. Notably, some catalysts with rather similar total carbide contents (5PFeCNF and 20PFeCNF) did exhibit rather different catalytic performances. This is in line with previous suppositions that carbide contents cannot account for differences in catalytic performance.[7]

DOI: 10.1021/acscatal.6b00131
ACS Catal. 2016, 6, 3147–3157

CH_4 Transient. Figure 1 illustrates typical normalized transient curves from a $^{13}CO/H_2/Kr$ to $^{12}CO/H_2/Ar$ back-switch. The overlap of the CO and Ar transients shows a low CO surface coverage (S3 in Supporting Information),[38,68,69] which suggests CO adsorption was dissociative. The response times for CH_4 are an order of magnitude longer in the case of Fe catalysts than for Co catalysts.[70] The two distinct gradients of decay observed for the CH_4 response time suggested the presence of two separate processes for methanation. To affirm this proposition and obtain a quantitative analysis, fitting of the CH_4 response curves to classic models from Soong et al. was performed (S4 in Supporting Information).[58,70] It was concluded that the parallel pools model provided the best fit. It is proposed that the fast pool relates to C atoms that stay at the surface of Fe carbide nanoparticles after CO dissociation, whereas the slow pool consists of C atoms that diffuse from the interior of the particles. Note that both pools react via the Mars–van-Krevelen-like mechanism.[47,48] Since the bulk C atoms can only react after they moved to the surface, analysis according to model D (the second pool being only a side-pool) seems most appropriate. The reported residence times are for the main (fast) pool, i.e., CH_x surface residence times (of species forming methane).

Figure 2 shows that, for unpromoted catalysts, increasing particle sizes did not result in significant changes in the surface residence times of CH_x present at the surface. This indicates that the intrinsic activity of active sites for methane formation ($k = 1/\tau_{CHx}$) was not considerably influenced by particle size if there were no promoters. However, for promoted catalysts, increasing particle sizes did lead to increasing CH_x surface residence times. This deviates from the previous work by Lohitharn and Goodwin who concluded that promoters do not influence intrinsic activity.[36,37]

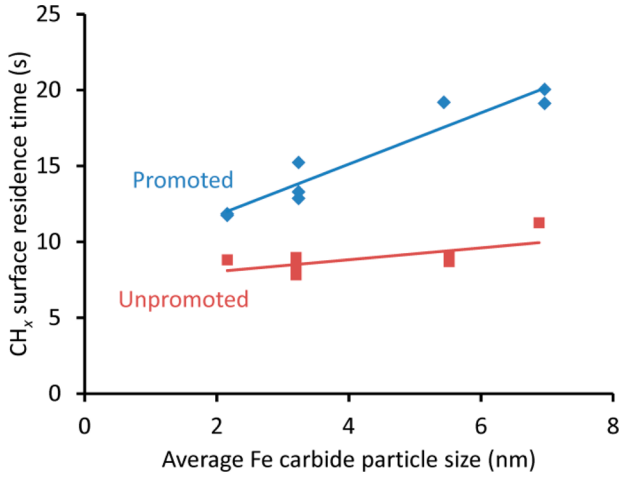

Figure 2. CH_x surface residence times (fast pool) obtained upon fitting to parallel side-pool model.

For both promoted and unpromoted catalysts, the CH_x coverage decreased upon increase in particle size (S4 in Supporting Information). This concurs with the hypothesis that there are a higher number of active sites at corners and edges, as these are more abundant on small iron carbide particles. Promoted catalysts recorded higher CH_x coverage in comparison to unpromoted catalysts, meaning that the presence of promoters apparently increased the number of active CH_x surface intermediates leading to hydrocarbon products.

Despite the lower intrinsic activity (for termination toward CH_4) per active site ($1/\tau_{CHx}$), the promoted catalysts showed higher overall activity (Table 2). This is an indication that the overall activity depended more on the number of CH_x surface intermediates than on the surface residence time of CH_x, and this is in agreement with literature results.[36,37] Figure 3 illustrates the relation between CH_x coverage and apparent turnover frequency (TOF). It appears that an increase in the number of active CH_x surface intermediates leads to a proportional increase in TOF.

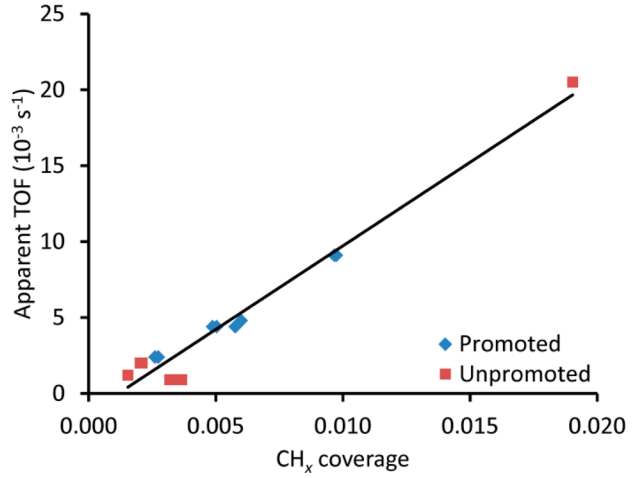

Figure 3. Apparent turnover frequency (TOF) as a function of CH_x surface coverages (350 °C, 1.85 bar, H_2/CO = 10).

On the other hand, CH_4 selectivity was independent of CH_x coverage (S4 in Supporting Information), which suggests that the methane selectivity relates to H coverage.

HD Transient. Figure 4 depicts typical normalized transient curves from a $CO/H_2/Kr$ to $CO/D_2/Ar$ switch, which was performed to determine H coverage. One of the observations is that the breakthrough of H_2 was much faster than Kr. This is attributed mainly to the faster diffusion rate of H_2 in comparison to Kr. As a result, H coverage could not be determined with the conventional data treatment. Instead, H coverage was determined using the formation of HD. The instantaneous HD formation indicates dissociative adsorption

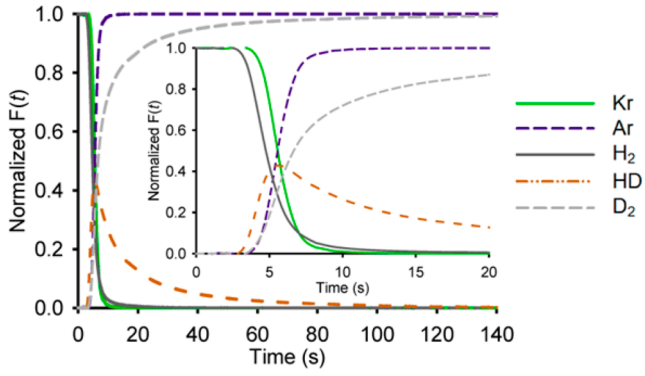

Figure 4. Typical normalized transient curves of full period and initial period (inset) from a $CO/H_2/Kr$ to $CO/D_2/Ar$ switch (catalyst 2PFeCNF).

DOI: 10.1021/acscatal.6b00131
ACS Catal. 2016, 6, 3147–3157

of H_2. The emergence of considerable tailing is proposed to involve H exchange with CH_x and OH_x species (also on CNF support).

The HD transient curves were fitted to newly derived equations for multiple pool systems, specifically derived for HD transients. The parallel side-pool model gave the best fits. To assess the accuracy of the fitted parameters, fits were also attempted with a numerical model including approximate corrections for curve broadening due to diffusion in the lines. Alternatively, only the peak of the HD curves was used to fit a single pool model. The results of these three fitting procedures led to the error bars drawn in Figures 5−7 (see also Supporting Information S5). With reference to Figure 5, an increase in particle size led to an increase in H surface residence times for the unpromoted catalysts. For the promoted catalysts, H surface residence times appeared to be rather independent of particle size.

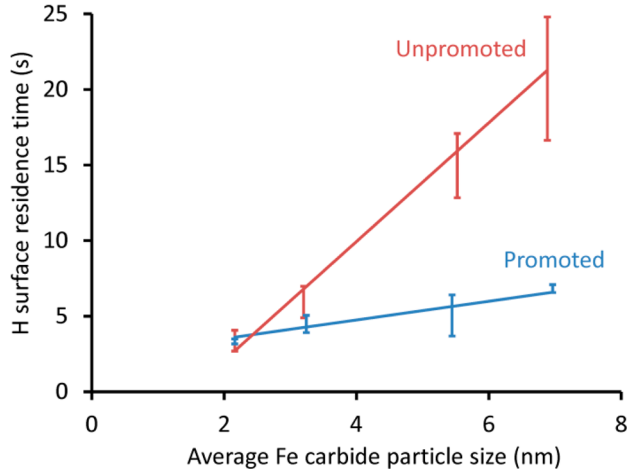

Figure 5. H surface residence times obtained upon fitting to parallel side-pool model. Error bars indicate the margin of uncertainty following from fitting different models.

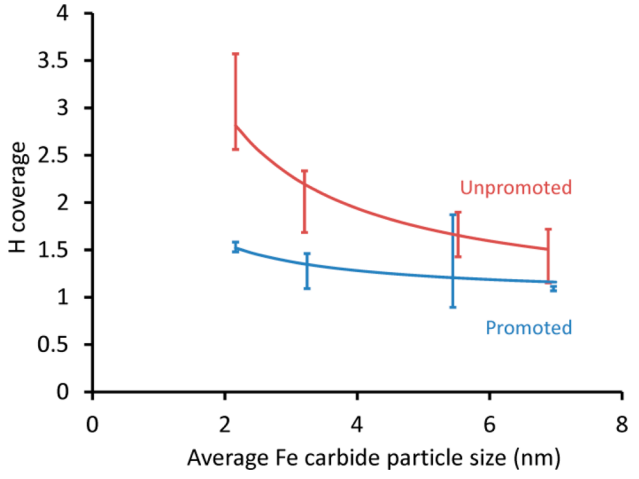

Figure 6. Hydrogen coverage after model fits as a function of Fe carbide particle size (350 °C, 1.85 bar, $H_2/CO = 10$). The trend line is drawn on the basis of consideration of edge and terrace sites (assuming constant coverages on edge and terrace sites regardless the particle size, which suggests that total coverage should be a function of the form $a + b/x$).

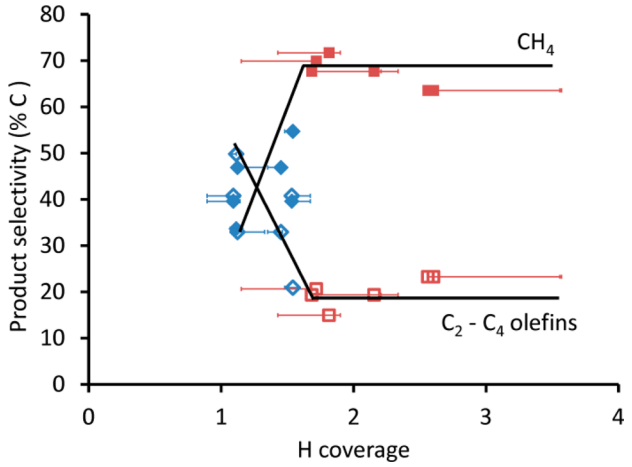

Figure 7. Product selectivity as a function of H coverage (350 °C, 1.85 bar, $H_2/CO = 10$): blue ◆ CH_4 and blue ◇ C_2−C_4 olefins selectivity for promoted catalysts; red ■ CH_4 and red □ C_2−C_4 olefins selectivity for unpromoted catalysts. Data points are for the parallel side-pool model while the error ranges include the diffusion and single-pool fits.

The comparison of H coverage for different particle sizes with and without promoters is presented in Figure 6. Upon increase in particle size, there was a decrease in H coverage. H coverages for promoted catalysts were lower than for unpromoted catalysts, which supports the proposition that hydrogenation is suppressed in the presence of promoters. It was noted that H coverages in all cases were above 1, which means that there was at least 1 H atom adsorbed per C surface atom. This is possible since 3 H atoms may be adsorbed on each C surface atom before CH_4 is formed.

Table 3 summarizes the coverages of catalysts obtained from isotopic switches at steady state. For the unpromoted catalysts, H was the dominant surface species, and the coverage of other species, such as CH_x and C_xH_y, was very low. Due to the abundance of H adsorbed on the surface, the C atoms produced will react with H atoms to methane, with limited opportunity for chain growth. On the other hand, for the promoted catalysts methanation is suppressed, especially in the case of larger particles, for which H coverage is lower. The lower H coverage also gives rise to olefins rather than paraffins being produced (Table 2).

Table 3. Average Surface Residence Times and Coverages of Catalysts Followed with Isotopic Switches at Steady State (1.85 bar, 350 °C, $H_2/CO = 10$, TOS = 20 h)

		CH_x coverage		H coverage	
	av Fe_5C_2 particle size (nm)	τ_{CHx} (s)	θ_{CHx}	$\tau_H{}^e$ (s)	$\theta_H{}^e$
2FeCNF	2.2	9	0.019	3	2.7
5FeCNF	3.2	9	0.001	5	2.1
10FeCNF	5.5	10	0.001	16	1.4
20FeCNF	6.9	13	0.002	25	1.2
2PFeCNF	2.2	12	0.010	4	1.6
5PFeCNF	3.2	13	0.005	5	1.4
10PFeCNF	5.4	19	0.006	5	1.3
20PFeCNF	7.0	20	0003	7	1.1

[e]Average H surface residence times and coverages obtained from parallel side-pool model.

DOI: 10.1021/acscatal.6b00131
ACS Catal. 2016, 6, 3147−3157

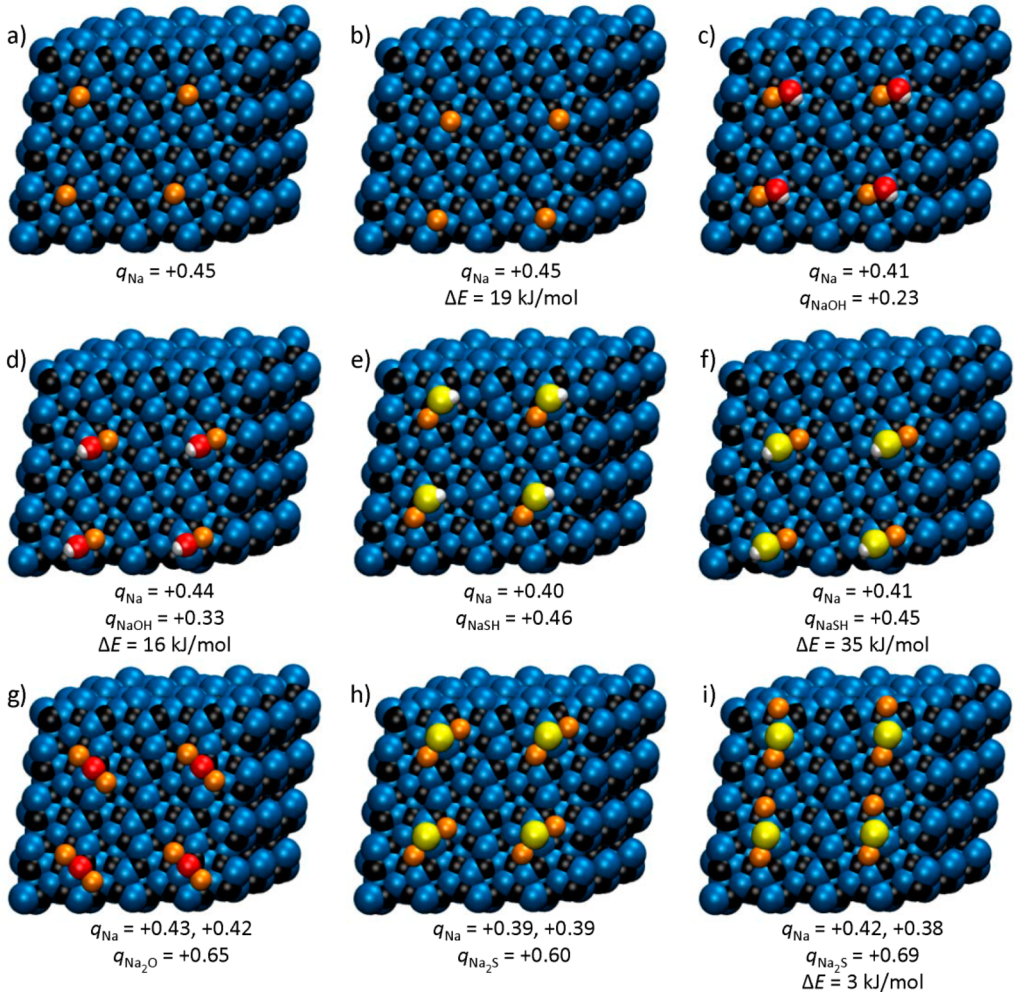

Figure 8. Energetically favorable positions and resulting charges of Na (a and b), NaOH (c and d), NaSH (e and f), Na_2O (g), and Na_2S (h and i) on the (111) surface of Fe_5C_2. For second most favorable positions (b, d, f, and i) also the energy difference with the most favorable position is given. Color coding: blue is Fe, black is C, ochre is Na, red is O, yellow is S, and white is H.

A relationship between H coverage and product selectivity is shown in Figure 7. For the promoted catalytic system, it is concluded that methane selectivity is directly proportional to H coverage while lower olefin selectivity is inversely proportional to H coverage. To understand the promoter effect on the selectivity further, DFT modeling was performed for H adsorption on promoted and unpromoted surfaces. Since the promoter effect on selectivity is strongest for large particles, this DFT study first focuses on terraces.

DFT Modeling. *Promoter Positions and Charges.* In the literature, often only Na or K atoms are studied as promoter species, but it seems unlikely that alkali metals are reduced at FT conditions. Hence, Na^+ should be studied including counterions. The most likely states are Na_2O and Na_2S, but for completeness we also studied NaOH and NaSH. The energetically favorable positions for the various promoter species on the Fe_5C_2 (111) surface are shown in Figure 8. It was found that the sodium atom maximizes its carbon contacts, leading to two favorable positions (Figure 8a,b), which differ in energy by 19 kJ/mol. The same two Na positions were found for NaOH and NaSH (Figure 8c–f). It is worth noticing that these favorable positions for sodium differ from the positions found for potassium.[71]

Interestingly, rather the same charge, q, was found for the sodium ion in all structures, including the sodium atom. This means that the atomically adsorbed sodium became fully ionic, donating its electron to the iron carbide surface. When there are counterions, though, part of this charge is taken by the counterions, and the donation to the surface decreases. This is especially true for NaOH and less so for NaSH since sulfur is less electronegative. For Na_2O versus Na_2S, this difference in charge going to the counterion instead of to the carbide surface is less pronounced due to different geometries. However, when Na_2O and Na_2S are optimized in the same geometries, it is again clear that oxygen takes a more negative charge than sulfur (in the geometry of Figure 8g, q_{Na2S} = +0.74; in the geometry of Figure 8h, q_{Na2O} = +0.51).

For Na_2O and Na_2S different favorable structures were found: oxygen binds on top of a carbon atom, while sulfur interacts with iron atoms. In fact, the oxygen of Na_2O forms a very short bond with the carbon of only 1.33 Å, which is longer than in a CO molecule but shorter than the single bond in, e.g., methanol. This explains the distorted charge donation to the surface.

Charges in Fe_5C_2 are not ionic but polar, with typical atomic charges at the surface of approximately +0.15 for Fe and −0.15 for C. As already stated in the literature, the effect of charge

DOI: 10.1021/acscatal.6b00131
ACS Catal. 2016, 6, 3147–3157

donation by the promoters is rather local:[53−55] typically, the charge on nearest neighbors of Na is lowered by 0.05−0.1 *e*, while on next-nearest neighbors the effect is at most 0.02 *e*, and on third nearest neighbors it is negligible.

Effect of Local Charges on H Adsorption. Since the SSITKA results suggest that the selectivity depends mostly on H coverage and availability, the focus is on H adsorption (Figure 9). H binds favorably on carbons, with the optimal

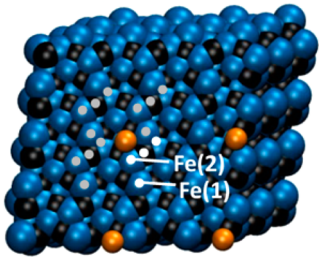

Figure 9. H positions that were studied (white dots). Due to the asymmetry introduced by 1 promoter species per 4 unit cells, there are 4 inequivalent duplicates of each position (gray dots), which are all studied. Color coding: blue is Fe, black is C, and ochre is Na.

position being on the same carbon that was found elsewhere to be the most active one for CH_x and CH_4 formation.[71] Adsorption on the other surface carbons (not shown in Figure 9) is weaker by 26, 33, and 44 kJ/mol, so these were not studied any further. This fits with the low CH_x coverages found with SSITKA: apparently, only a fraction of the available carbons are active. Placing the H on Fe atoms, there are two Fe positions preferred over the rest of the Fe sites, however with negative binding energy with respect to gaseous H_2. Alternatively, H can bind on the empty surface by bridging between two iron atoms with intermediate adsorption energies. However, on promoted surfaces this becomes less stable than binding atop.

When these H positions and their inequivalent duplicates were studied on the promoted surfaces, an excellent correlation was found with the atomic charges of the accepting Fe or C (Figure 10). The more negative charge promoters donate to an iron atom, the stronger the adsorption of H on that iron atom becomes. Note that on Fe(2) the H adsorption is more sensitive to this promoter effect than on Fe(1), which means that the effect apparently is quantitatively different for different local geometries. For different Fe_5C_2 surfaces a different sensitivity can be expected as well.

For the energetically second most favorable NaOH and NaSH structures (Figure 8d,f), upon H adsorption at Fe(2), the sodium ion tends to move somewhat toward the adsorbing H. As a result, the charge donation to this iron increases, and the H adsorption is strengthened even more, explaining the outliers in Figure 10. The outliers for Fe(1) are for the same NaSH structure, but in this case no explanation was found.

On a side note, the adsorption energies in Figure 10 are rather low for a process that is run at 350 °C. This is related to the choice of the rPBE functional: In general, the PBE functional gives too strong an adsorption, so the rPBE functional was developed to correct for this.[63] Typically, this gives a lowering in adsorption energies of roughly 60 kJ/mol. For weak adsorbates, however, that may be too much, leading to overcorrection.

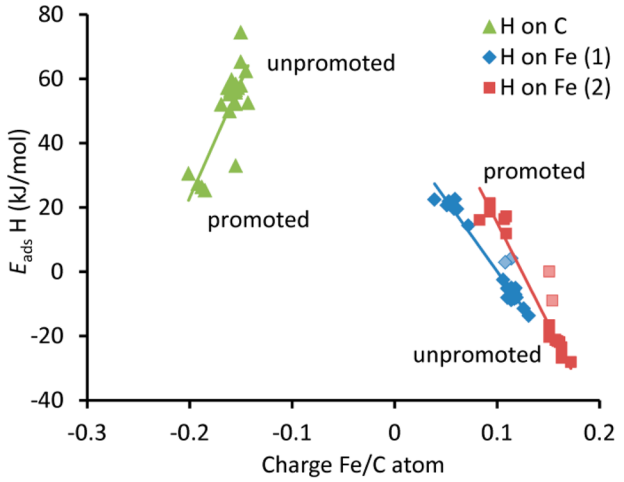

Figure 10. Effect of local charges on H adsorption: Negative charge donated to the Fe_5C_2 surface increases the H adsorption strength on top of Fe atoms, but weakens the bonding to C atoms. Fe(1) and Fe(2) denote the two different Fe sites. Outliers are colored lighter and are explained in the main text. E_{ads} H is defined with respect to $1/2H_2(g)$.

For adsorption on carbon, we see the opposite effect compared to that on iron: negative charge donation from the promoter species makes H adsorption on carbon weaker. We conclude that this is the determining factor for the improved selectivity caused by adding promoters: Due to charge donation to the Fe_5C_2 surface, the equilibrium between hydrogens staying on Fe or binding with carbon changes in favor of staying on Fe. This results in less methane formation and more β-H removal leading to olefin formation. With respect to chain growth probabilities, it should be realized that while termination to alkanes is decreased, the β-H removal termination increases, so there could be little net effect on chain growth probabilities for C_{2+} compounds.

Differences between Promoters. In a comparison among the different promoter species studied (Figure 11), the effect on

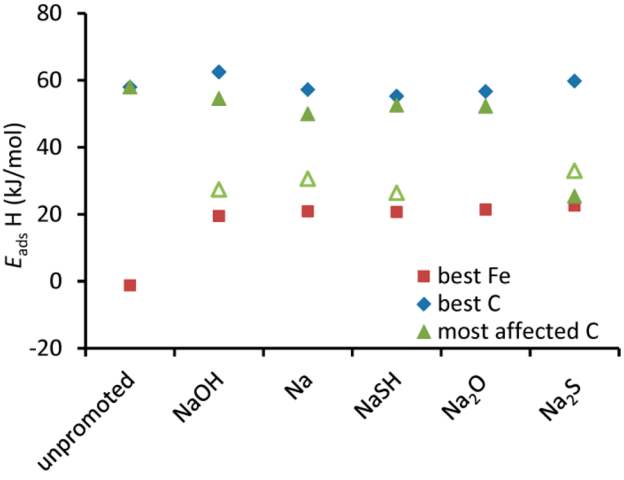

Figure 11. Comparison between promoter species. Results for second-most favorable promoter positions are denoted by open symbols, showing that the two Na positions have rather different effects on the studied carbons. Na_2S is the only promoter for which the actual (favorable) promoter position has a strong effect on H adsorption on carbon.

DOI: 10.1021/acscatal.6b00131
ACS Catal. 2016, 6, 3147−3157

adsorption to Fe is similar between promoters, since there is always an Fe site with a Na neighbor. The adsorption on C is more interesting: For the most affected C, a complicated trend is found that is determined by exact geometries. For the preferred Na position, the charge effect on the active carbons is limited, while for the second-most favorable Na position the effect is much larger. Interestingly, Na_2S combines these two positions and has a strong effect in its preferred geometry as well. Na_2O also combines the two Na positions, but the oxygen blocks the carbon it sits on, and the closest active carbon is far away and hardly affected. This may explain the superior qualities of Na_2S compared to those of the other promoter species studied here.

However, since we have 4 inequivalent duplicates of the active carbon atom (Figure 9), hydrogens can choose to go to one that is hardly affected. Therefore, it is important that the promoter concentration is high enough that there are Na neighbors at all active carbons. To confirm this, we modeled a doubled concentration of 2 promoter species per 4 unit cells for Na_2O and Na_2S (Figure 12). Besides the different local

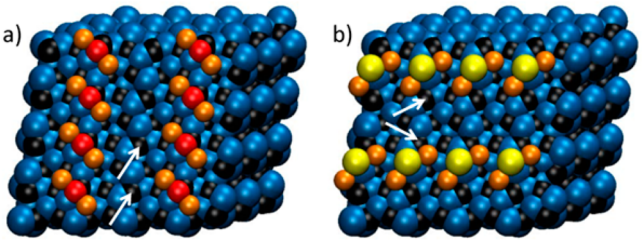

Figure 12. Optimized structures for 2 Na_2O (a) or 2 Na_2S (b) species per 4 unit cells. With 2 Na_2O species, still active carbons with no Na neighbor exist; with 2 Na_2S species, all active carbons have a Na neighbor. Color coding: blue is Fe, black is C, ochre is Na, red is O, and yellow is S.

geometry, also the pattern over the surface differs between these promoters, again in favor of Na_2S. For Na_2S, now all active carbon atoms have a direct Na neighbor, stimulating the preferred selectivity.

The results are summarized in Figure 13. Promoters decrease the energy of hydrogen atoms on iron sites (increasing the bond strength) but increase the energy on carbon sites (decreasing the bond strength). This lowers the H coverage on carbon, as was found with the SSITKA work, and lowers the selectivity toward methane. In a comparison among different sites around the Na_2S species, the effects vary, but on all positions either the binding on iron has strengthened or the binding on carbon has weakened, leading to similar shifts in the equilibrium away from methane formation. Hence, on unpromoted Fe_5C_2 it seems H_2 will split on iron sites and immediately move to the active carbon positions, forming CH_x and ultimately CH_4. On promoted surfaces the hydrogens have a much greater chance to come back off the carbon, as witnessed by higher olefin formation, lower H coverage, and shorter H residence times.

Throughout this discussion it should be realized that the amounts of Na_2S versus Na_2O depend on the ratio Na:S on the particle surface. Typically most of the sodium resides on the support, and only the rest sits on the particles. When this amount exceeds the stoichiometric amount of sulfur, both Na_2O and Na_2S will be formed. Note that the ratio between

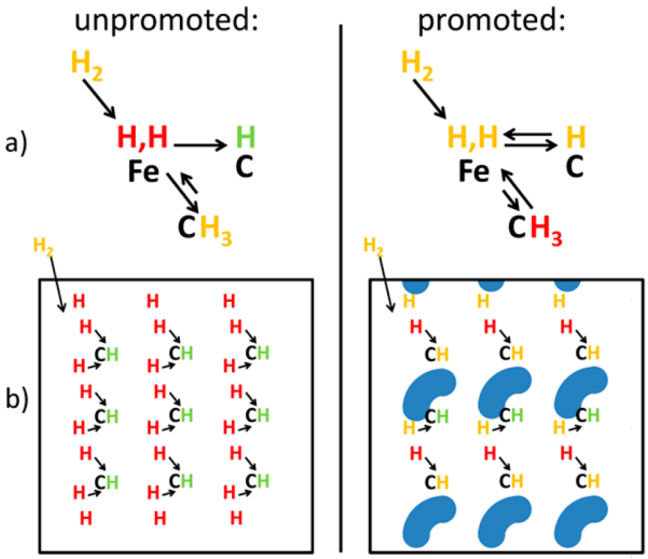

Figure 13. Cartoon of promoter effect by Na_2S. Colors of hydrogen atoms denote their energy: red, yellow, and green denote high, medium, and low energy, respectively. The blue shapes denote the Na_2S species. (a) The promoter increases the H adsorption strength on iron and decreases the adsorption on carbon, thereby decreasing methane formation and increasing olefin formation. (b) The strength of the effect differs per site, but at both sites the equilibrium between binding to iron or carbon is shifted.

support and particle surface varies with the iron loading and particle size, so the optimal ratio Na:S will also vary.[72]

As a final remark, Na_2O and Na_2S may react with product H_2O to form 2 NaOH or NaOH + NaSH, respectively. According to Figure 11, this would remove the advantage of having sulfur, since NaSH is less effective than Na_2S. Na_2O and NaOH are equally ineffective. For Na_2O, this reaction is rather likely with a ΔE of −62 kJ/mol (comparing H_2O adsorbed on top of adsorbed Na_2O plus an empty surface with 2 adsorbed NaOH species); for Na_2S this is much less likely with a ΔE of −4 kJ/mol. Still this suggests again that high promoter coverages should be preferred to favor the presence of Na_2S species over NaSH and NaOH formation.

CONCLUSION

The fundamentals of iron particle size and promoter effects on FTO catalysis were studied. Previously, it was found under industrially relevant conditions that increasing particle size lowers the apparent turnover frequency. The selectivity, however, increases with increasing particle size, but interestingly, this only happens when promoters (Na plus S) are present.[7] In the present paper we show that these trends also hold under the methanation conditions needed to perform a SSITKA study.

Following the isotopic switch from ^{13}CO to ^{12}CO, coverages and residence times of CO and CH_x were investigated. Extremely low CO coverage was observed for all catalysts, suggesting dissociative adsorption of CO. The two distinct gradients of the CH_4 response curves fitted well to a parallel pool model, interpreted as a main-pool of surface carbon and a side-pool of carbon atoms that diffuse from the interior of the carbide nanoparticles. For both promoted and unpromoted catalysts, CH_x coverage decreased with increasing particle size. This is tentatively assigned to the fact that smaller particles have a higher number of highly active low coordination sites, which

DOI: 10.1021/acscatal.6b00131
ACS Catal. 2016, 6, 3147−3157

are presumably sites for C−H bond formation. CH_x surface residence times suggest that CH_4 formation occurs equally fast on edges and terraces for unpromoted catalysts, but is slowed down on the terraces of promoted catalysts. The turnover frequency was established to be directly proportional to the CH_x coverage.

Isotopic switching from H_2 to D_2 was carried out to study the H coverage and residence times. HD response curves were fitted to various models derived from ref 58. The estimated H coverage was shown to decrease upon promoter addition, which gives rise to less termination via hydrogen addition and thereby lower methane selectivities. H coverage appeared to decrease with increasing particle size, which indicated that H atoms are more abundant at corners and edges. H coverage displayed a negative correlation with lower olefin selectivity but a positive correlation with methane selectivity. This strongly suggests that hydrogen coverage is a vital factor influencing product selectivity for FTO.

In order to comprehend the promoter's influence on H coverage, DFT modeling was performed. In a comparison of Na, NaOH, NaSH, Na_2O, and Na_2S promoter species, the counterions were shown to draw away some of the charge that the Na otherwise donates to the iron carbide surface. As S is less electronegative than O, it draws less charge away from the Fe_5C_2 surface, making Na_2S a better promoter than Na_2O. Also, the binding modes of Na_2S and Na_2O differ, which turns out to be an even more important factor in favor of Na_2S.

H adsorption on the Fe_5C_2 surface was subsequently calculated, and H was found to bind preferably to C. On promoted Fe_5C_2, H adsorption was shown to correlate with the atomic charge of the accepting Fe or C. When negative charge donation from the promoter species increases, H adsorption becomes stronger on Fe and weaker on C. Thus, while on unpromoted Fe_5C_2 surfaces H atoms bind preferably on C after dissociation on Fe, on promoted Fe_5C_2 surfaces the difference between adsorption on Fe or C becomes smaller. This results in less methane formation and more β-H removal leading to olefin formation.

■ ASSOCIATED CONTENT

Supporting Information

The Supporting Information is available free of charge on the ACS Publications website at DOI: 10.1021/acscatal.6b00131.

Catalyst characterization, catalytic performance at methanation condition, CO response curves, CH_x response curves, and HD response curves (PDF)
DFT coordinates (XYZ)

■ AUTHOR INFORMATION

Corresponding Authors

*E-mail: K.P.deJong@uu.nl.
*E-mail: M.J.Louwerse@uu.nl.

Present Address

[‖]SINTEF Materials and Chemistry, N-7463 Trondheim, Norway.

Notes

The authors declare no competing financial interest.

■ ACKNOWLEDGMENTS

This research received funding from The Netherlands Organization for Scientific Research (NWO) in the framework of the TASC Technology Area "Syngas, a Switch to Flexible New Feedstock for the Chemical Industry (TA-Syngas)". Dow and Johnson Matthey are also acknowledged for the funding received. C. van de Spek and I. Springer are thanked for the TEM images and ICP elemental analysis, respectively. H. M. Torres Galvis, M. Ruitenbeek, A. C. J. Koeken, M. Watson, and Leon van de Water are thanked for fruitful discussion. Arjan den Otter is acknowledged for the remeasurement of a sample. The modeling work was funded by the Dutch National Research School Combination Catalysis (NRSC-C).

■ REFERENCES

(1) Wildgoose, G. G.; Banks, C. E.; Compton, R. G. *Small* **2006**, *2* (2), 182−193.
(2) White, R. J.; Luque, R.; Budarin, V. L.; Clark, J. H.; Macquarrie, D. J. *Chem. Soc. Rev.* **2009**, *38* (2), 481−494.
(3) Nørskov, J. K.; Bligaard, T.; Hvolbaek, B.; Abild-Pedersen, F.; Chorkendorff, I.; Christensen, C. H. *Chem. Soc. Rev.* **2008**, *37* (10), 2163−2171.
(4) McCue, A. J.; Anderson, J. A. *Catal. Sci. Technol.* **2014**, *4* (2), 272−294.
(5) Bezemer, G. L.; Bitter, J. H.; Kuipers, H. P. C. E.; Oosterbeek, H.; Holewijn, J. E.; Xu, X.; Kapteijn, F.; van Dillen, A. J.; de Jong, K. P. *J. Am. Chem. Soc.* **2006**, *128* (12), 3956−3964.
(6) Kang, J.; Zhang, S.; Zhang, Q.; Wang, Y. *Angew. Chem., Int. Ed.* **2009**, *48* (14), 2565−2568.
(7) Torres Galvis, H. M.; Bitter, J. H.; Davidian, T.; Ruitenbeek, M.; Dugulan, A. I.; de Jong, K. P. *J. Am. Chem. Soc.* **2012**, *134* (39), 16207−16215.
(8) Torres Galvis, H. M.; de Jong, K. P. *ACS Catal.* **2013**, *3* (9), 2130−2149.
(9) Iglesia, E. *Appl. Catal., A* **1997**, *161* (1−2), 59−78.
(10) Ren, T.; Patel, M.; Blok, K. *Energy* **2006**, *31* (4), 425−451.
(11) Rahimi, N.; Karimzadeh, R. *Appl. Catal., A* **2011**, *398* (1−2), 1−17.
(12) Vispute, T. P.; Zhang, H.; Sanna, A.; Xiao, R.; Huber, G. W. *Science* **2010**, *330* (6008), 1222−1227.
(13) Higman, C.; Tam, S. *Chem. Rev.* **2014**, *114* (3), 1673−1708.
(14) Guo, X.; Fang, G.; Li, G.; Ma, H.; Fan, H.; Yu, L.; Ma, C.; Wu, X.; Deng, D.; Wei, M.; Tan, D.; Si, R.; Zhang, S.; Li, J.; Sun, L.; Tang, Z.; Pan, X.; Bao, X. *Science* **2014**, *344* (6184), 616−619.
(15) Lanzafame, P.; Centi, G.; Perathoner, S. *Chem. Soc. Rev.* **2014**, *43* (22), 7562−7580.
(16) McCann, D. M.; Lesthaeghe, D.; Kletnieks, P. W.; Guenther, D. R.; Hayman, M. J.; Van Speybroeck, V.; Waroquier, M.; Haw, J. F. *Angew. Chem., Int. Ed.* **2008**, *47* (28), 5179−5182.
(17) Olsbye, U.; Svelle, S.; Bjørgen, M.; Beato, P.; Janssens, T. V. W.; Joensen, F.; Bordiga, S.; Lillerud, K. P. *Angew. Chem., Int. Ed.* **2012**, *51* (24), 5810−5831.
(18) Cai, G.; Liu, Z.; Shi, R.; Changing, H.; Yang, L.; Sun, C.; Chang, Y. *Appl. Catal., A* **1995**, *125* (1), 29−38.
(19) Janardanarao, M. *Ind. Eng. Chem. Res.* **1990**, *29* (9), 1735−1753.
(20) Khodakov, A. Y.; Chu, W.; Fongarland, P. *Chem. Rev.* **2007**, *107* (5), 1692−1744.
(21) de Smit, E.; Weckhuysen, B. M. *Chem. Soc. Rev.* **2008**, *37* (12), 2758−2781.
(22) Zhang, Q.; Kang, J.; Wang, Y. *ChemCatChem* **2010**, *2* (9), 1030−1058.
(23) Bromfield, T. C.; Coville, N. J. *Appl. Catal., A* **1999**, *186* (1−2), 297−307.
(24) Ngantsoue-Hoc, W.; Zhang, Y.; O'Brien, R. J.; Luo, M.; Davis, B. H. *Appl. Catal., A* **2002**, *236* (1−2), 77−89.
(25) Huo, C.-F.; Wu, B.-S.; Gao, P.; Yang, Y.; Li, Y.-W.; Jiao, H. *Angew. Chem., Int. Ed.* **2011**, *50* (32), 7403−7406.
(26) Graf, B.; Muhler, M. *Phys. Chem. Chem. Phys.* **2011**, *13* (9), 3701−3710.
(27) Schulte, H. J.; Graf, B.; Xia, W.; Muhler, M. *ChemCatChem* **2012**, *4* (3), 350−355.

DOI: 10.1021/acscatal.6b00131
ACS Catal. 2016, 6, 3147−3157

(28) Xiong, H.; Motchelaho, M. A.; Moyo, M.; Jewell, L. L.; Coville, N. J. *Appl. Catal., A* **2014**, *482*, 377−386.
(29) Lu, J.; Yang, L.; Xu, B.; Wu, Q.; Zhang, D.; Yuan, S.; Zhai, Y.; Wang, X.; Fan, Y.; Hu, Z. *ACS Catal.* **2014**, *4* (2), 613−621.
(30) Torres Galvis, H. M.; Bitter, J. H.; Khare, C. B.; Ruitenbeek, M.; Dugulan, A. I.; de Jong, K. P. *Science* **2012**, *335* (6070), 835−838.
(31) Torres Galvis, H. M.; Koeken, A. C. J.; Bitter, J. H.; Davidian, T.; Ruitenbeek, M.; Dugulan, A. I.; de Jong, K. P. *J. Catal.* **2013**, *303*, 22−30.
(32) Shannon, L.; Goodwin, J. G. *Chem. Rev.* **1995**, *95* (3), 677−695.
(33) Ledesma, C.; Yang, J.; Chen, D.; Holmen, A. *ACS Catal.* **2014**, *4* (12), 4527.
(34) Jacobs, G.; Davis, B. H. *Catal. Sci. Technol.* **2014**, *4* (11), 3927−3944.
(35) Sudsakorn, K.; Goodwin, J. G.; Adeyiga, A. A. *J. Catal.* **2003**, *213* (2), 204−210.
(36) Lohitharn, N.; Goodwin, J. G., Jr. *J. Catal.* **2008**, *257* (1), 142−151.
(37) Lohitharn, N.; Goodwin, J. G., Jr. *Catal. Commun.* **2009**, *10* (6), 758−762.
(38) Govender, N. S.; Botes, F. G.; de Croon, M. H. J. M.; Schouten, J. C. *J. Catal.* **2008**, *260* (2), 254−261.
(39) Govender, N. S.; de Croon, M. H. J. M.; Schouten, J. C. *Appl. Catal., A* **2010**, *373* (1−2), 81−89.
(40) Govender, N. S.; Botes, F. G.; de Croon, M. H. J. M.; Schouten, J. C. *J. Catal.* **2014**, *312*, 98−107.
(41) Ojeda, M.; Nabar, R.; Nilekar, A. U.; Ishikawa, A.; Mavrikakis, M.; Iglesia, E. *J. Catal.* **2010**, *272* (2), 287−297.
(42) van Santen, R. A.; Ghouri, M. M.; Shetty, S.; Hensen, E. M. H. *Catal. Sci. Technol.* **2011**, *1* (6), 891−911.
(43) van Santen, R. A.; Markvoort, A. J.; Filot, I. A. W.; Ghouri, M. M.; Hensen, E. J. M. *Phys. Chem. Chem. Phys.* **2013**, *15* (40), 17038−17063.
(44) Steynberg, P. J.; van den Berg, J. A.; van Rensburg, W. J. *J. Phys.: Condens. Matter* **2008**, *20* (6), 064238−064249.
(45) Zhao, S.; Liu, X.-W.; Huo, C.-F.; Li, Y.-W.; Wang, J.; Jiao, H. *J. Catal.* **2012**, *294*, 47−53.
(46) de Smit, E.; Cinquini, F.; Beale, A. M.; Safonova, O. V.; van Beek, W.; Sautet, P.; Weckhuysen, B. M. *J. Am. Chem. Soc.* **2010**, *132* (42), 14928−14941.
(47) Gracia, J. M.; Prinsloo, F. F.; Niemantsverdriet, J. W. *Catal. Lett.* **2009**, *133* (3−4), 257−261.
(48) Ozbek, M. O.; Niemantsverdriet, J. W. *J. Catal.* **2015**, *325*, 9−18.
(49) Cao, D.; Zhang, F.-Q.; Li, Y.-W.; Wang, J.; Jiao, H. *J. Phys. Chem. B* **2005**, *109* (21), 10922−10935.
(50) Sorescu, D. C. *J. Phys. Chem. C* **2009**, *113* (21), 9256−9274.
(51) Petersen, M. A.; van den Berg, J.; van Rensburg, W. J. *J. Phys. Chem. C* **2010**, *114* (17), 7863−7879.
(52) Pham, T. H.; Duan, X.; Qian, G.; Zhou, X.; Chen, D. *J. Phys. Chem. C* **2014**, *118* (19), 10170−10176.
(53) Huo, C.-F.; Li, Y.-W.; Wang, J.; Jiao, H. *J. Am. Chem. Soc.* **2009**, *131* (41), 14713−14721.
(54) Sorescu, D. C. *Surf. Sci.* **2011**, *605* (3−4), 401−414.
(55) Petersen, M. A.; Cariem, M. J.; Claeys, M.; van Steen, E. *Appl. Catal., A* **2015**, *496*, 64−72.
(56) van der Lee, M. K.; van Dillen, A. J.; Geus, J. W.; de Jong, K. P.; Bitter, J. H. *Carbon* **2006**, *44* (4), 629−637.
(57) Frøseth, V.; Storsæter, S.; Borg, Ø.; Blekkan, E. A.; Rønning, M.; Holmen, A. *Appl. Catal., A* **2005**, *289* (1), 10−15.
(58) Soong, Y.; Krishna, K.; Biloen, P. *J. Catal.* **1986**, *97*, 330−343.
(59) Ding, M.; Yang, Y.; Wu, B.; Wang, T.; Ma, L.; Xiang, H.; Li, Y. *J. Mol. Catal. A: Chem.* **2011**, *351*, 165−173.
(60) Pendyala, V. R. R.; Graham, U. M.; Jacobs, G.; Hamdeh, H. H.; Davis, B. H. *ChemCatChem* **2014**, *6* (7), 1952−1960.
(61) te Velde, G.; Bickelhaupt, F. M.; Baerends, E. J.; Fonseca Guerra, C.; van Gisbergen, S. J. A.; Snijders, J. G.; Ziegler, T. *J. Comput. Chem.* **2001**, *22* (9), 931−967.
(62) Fonseca Guerra, C.; Visser, O.; Snijders, J. G.; te Velde, G.; Baerends, E. J. *Methods and Techniques for Computational Chemistry*; Clementi, E., Corongiu, C., Eds.; STEF: Cagliari, 1995.
(63) Hammer, B.; Hansen, L. B.; Nørskov, J. K. *Phys. Rev. B: Condens. Matter Mater. Phys.* **1999**, *59* (11), 7413−7421.
(64) Grimme, S.; Antony, J.; Ehrlich, S.; Krieg, H. *J. Chem. Phys.* **2010**, *132* (15), 154104−154119.
(65) Grimme, S.; Ehrlich, S.; Goerigk, L. *J. Comput. Chem.* **2011**, *32*, 1456−1465.
(66) Zhao, S.; Liu, X.-W.; Huo, C.-F.; Li, Y.-W.; Wang, J.; Jiao, H. *Catal. Struct. React.* **2015**, *1* (1), 44−60.
(67) Hirshfeld, F. L. *Theor. Chim. Acta* **1977**, *138* (44), 129−138.
(68) Mims, C. A.; McCandlish, L. E. *J. Am. Chem. Soc.* **1985**, *107*, 696−697.
(69) Mims, C. A.; McCandlish, L. E. *J. Phys. Chem.* **1987**, *91* (4), 929−937.
(70) den Breejen, J. P.; Radstake, P. B.; Bezemer, G. L.; Bitter, J. H.; Frøseth, V.; Holmen, A.; de Jong, K. P. *J. Am. Chem. Soc.* **2009**, *131* (20), 7197−7203.
(71) Zhao, S.; Liu, X.-W.; Huo, C.-F.; Li, Y.-W.; Wang, J.; Jiao, H. *Appl. Catal., A* **2015**, *493*, 68−76.
(72) Zhou, X.; Ji, J.; Wang, D.; Duan, X.; Qian, G.; Chen, D.; Zhou, X. *Chem. Commun.* **2015**, *51* (42), 8853−8856.

DOI: 10.1021/acscatal.6b00131
ACS Catal. 2016, 6, 3147−3157